Electronic and Structural Evidences for Charge Transfer and Localization in Iodine-Doped Pentacene

M. Brinkmann,* V. S. Videva,† A. Bieber, J. J. André, and P. Turek

Institut Charles Sadron, UPR 22, CNRS, 6 rue Boussingault, BP 40016, F-67083 Strasbourg Cedex, France

L. Zuppiroli,* P. Bugnon, M. Schaer, and F. Nuesch

Laboratoire d'optoélectronique des matériaux moléculaires, Institut des matériaux, Ecole Polytechnique, CH-1015 Lausanne, Switzerland

R. Humphry-Baker

Laboratoire de photonique et interfaces, Institut de chimie moléculaire et biologique, Ecole Polytechnique, CH-1015 Lausanne, Switzerland

Received: April 15, 2004; In Final Form: July 5, 2004

We have investigated the doping mechanism of pentacene with iodine and its impact on the structure and on the electronic properties of single crystals, powders, and thin films in a large range of iodine concentration up to six iodine per pentacene (PEN) molecule (I/PEN = 6). Three regimes of doping have been identified. In the low doping regime I/PEN < 0.05, the pristine pentacene structure of single crystals is maintained. Electron spin resonance (ESR) evidences a Pauli susceptibility, that is, the characteristic fingerprint of delocalized holes in the valence band of pentacene. In the intermediate doping regime (0.1 < I/PEN ≤ 2.0), iodine diffuses between the (*a*,*b*) planes of the pentacene structure and forms an intercalate. Charge transfer between iodine and pentacene is witnessed by both UV−vis and IR signatures of PEN^+ cations and related species, for example, cation dimers $(PEN^+)_2$ and typical Raman signatures of the I_3^- and I_5^- species. Spin pairing of pentacene cation radicals is further supported by the observation of a thermally activated behavior of the ESR spin susceptibility. In the heavy doping regime (2 < I/PEN ≤ 6), all traces of structural order vanish, indicating that iodine penetrates within the (*a*,*b*) planes of the intercalate in a disordered manner, forming an amorphous-like material. This high degree of disorder results in increased charge localization. Most spin/charge species are ESR-silent and only a limited fraction (a few percents) exhibits a Curie-like susceptibility. Because of disorder, the macroscopic conductivity of doped pentacene single crystals does not exceed a few S/cm at 300 K.

I. Introduction

Since the work of Karl et al.,[1] pentacene is well known to be a good molecular semiconductor with hole mobilities of several hundreds $cm^2/V \cdot s$ at low temperatures. It is thus natural to try to associate this weak donor molecule with an acceptor, such as iodine, to induce charge transfer and electronic conduction. These experiments were successful with other donor molecules such as perylene,[2,3] nickel phthalocyanine,[4,5] copper phthalocyanine,[6] tetrathiofulvalene (TTF),[7] and related compounds,[8] tetrathiotetracene (TTT) based materials[9] and, of course, conjugated polymers (which act both as donors and acceptors). A review on these subjects can be found in the book by one of us.[10]

In iodine-doped organic semiconductors, only under specific circumstances corresponding to a well-defined stoichiometry, does the polyiodide phase organize together with the donor lattice and form a radical-ion salt. Several examples of this ordered behavior can be found in ref 10, including copper phthalocyanine-iodide (CuPcI) and nickel phthalocyanine-iodide (NiPcI) which are model materials in this respect.[3,4] In this case, one can obtain massive charge transfer from the donor to the acceptor lattice and "true" metallic conductivity. However, the doping procedure from the vapor phase does not usually lead to highly crystalline samples; the polyiodide phase remains disordered and the opportunities of charge transfer are limited to a few percent of the donor molecules. Pentacene, iodine-doped from the vapor phase, enters this last category.

For pentacene, a few experiments performed on polycrystalline films, powders, and amorphous films doped with iodine have already been published.[11−14] They showed that, in the first stages of doping, the structure of pentacene is not changed too much, in such a way that iodine intercalates between the (*a*,*b*) layers of pentacene molecules.[11] Electron spin resonance (ESR) experiments were also carried out in iodine[13,14] as well as in alkaline-doped pentacene[15−18] (potassium and rubidium) which showed that two undefined types of spins are present on the pentacene lattice because of charge transfer. They also demonstrated that ohmic conductivities about 10−100 S/cm at room temperature result from the iodine as well as from the alkaline doping.

The aim of the present study is to understand the overall doping mechanism of pentacene by iodine over a large range of composition (0.05 ≤ I/Pen ≤ 6). The manuscript has been

* Corresponding authors. E-mail: brinkman@ics.u-strasbg.fr; libero.zuppiroli@epfl.ch.

† Present address: Department of Analytical Chemistry, Faculty of Chemistry, Sophia University, 1164 Sophia, Japan.

10.1021/jp048343x CCC: $27.50
Published on Web 09/14/2004

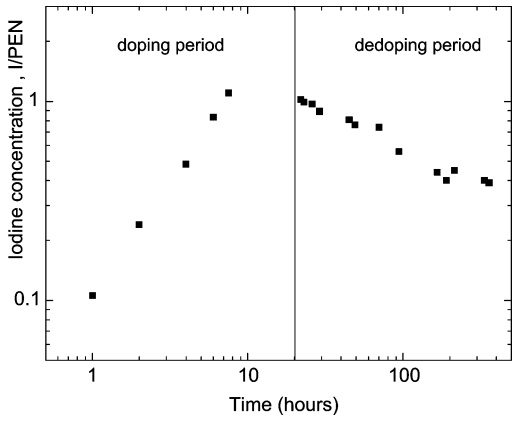

Figure 1. Doping and dedoping of a pentacene single crystal in ambient atmosphere and iodine vapor. The iodine concentration was obtained from weight measurements.

organized in the following manner: Section II is dedicated to the description of the doping procedure, the samples, and the various methods used for the study of the structure, spectroscopic, magnetic, and transport properties. Section III is dedicated to the experimental results. We first discuss the evidences for charge transfer obtained from the spectroscopic and the structural points of view and subsequently present the impact of doping on the magnetic and transport properties as a function of iodine concentration in the samples.

II. Experimental Section

1. Sample Preparation. Pentacene powder was purchased from Aldrich and purified twice by gradient sublimation before use. Single crystals were grown by vapor transport of pentacene under a thermal gradient. To this aim, the purified pentacene powder was sealed in a glass tube filled with a gas mixture including hydrogen. Oriented pentacene thin films were grown on oriented poly(tetrafluoroethylene) (PTFE) substrates by high vacuum sublimation using a Kurt−Lesker evaporator system at a base pressure of 4×10^{-7} mbar and deposition rate of 1 nm/min. Experimental conditions used to prepare the substrates are presented elsewhere.[19]

The X-ray diffractograms of powders and single crystals exhibit the $d_{001} = 14.15$ Å reflection which is characteristic of the bulk polymorph with a triclinic structure previously identified in the literature.[20] Thin films grown onto oriented PTFE substrates with a substrate temperature $T_s \geq 65$ °C give rise to the bulk polymorph characterized by $d_{001} = 14.5$ Å which has also been identified by transmission electron microscopy.[19]

2. Doping Procedures. The samples were doped in three different manners: (i) from a pure saturated vapor of iodine, that is, after preliminary degasing of the samples (powders and single crystals), (ii) by using a mixture with an inert gas (single crystals), or (iii) in mixture of iodine vapor and ambient atmosphere (thin films). In powders or single crystals, the iodine concentration in the sample was deduced from the weight of the sample before and after doping. In films or single crystals, the doping was monitored by the growth of the electron spin resonance (ESR) signal. When concentrations are given in the text or in the figures, they always result from a direct weighting. In the other cases, only the doping period is indicated and the concentration is determined indirectly. The control of the doping process from the vapor phase is rather difficult. The lack of control of the homogeneity of the sample could result in misinterpretations of the experimental data. The present work has considered these kinetic problems carefully. Figure 1 gives an example of the absorption−desorption process in a single crystal of 1.3 mg. In this typical case, the doping kinetics at 293 K involves times about 10−100 h. In situ ESR experiments have also shown that the homogeneity of a single crystal of a few hundreds of nm thick, with respect to the dopant concentration, involves dedoping times at 293 K of approximately 10 h.

The stability of the doped samples depends on the composition. For I/PEN ≥ 4, the material is stable at 293 K, while in the intermediate range $1 \leq$ I/PEN ≤ 3, one-third of the iodine content is desorbed within times of about 10 h or more. This observation is very similar to the case of perylene·$I_{2.92}$.[2,3]

3. Spectroscopic Characterization. Optical spectroscopy in the UV−vis was performed on a Varian Cary 50 spectrophotometer. The pentacene film onto oriented PTFE (0.8×3 cm^2) was placed in a quartz cell. Conductivity was measured simultaneously on the sample between two gold electrodes deposited on top of the PTFE/glass substrate (500-μm interdigit spacing) using a Keithley 2400 electrometer. At time $t = 0$, an iodine grain (0.5 mg) was dropped in the quartz cell which was subsequently closed and the iodine vapor progressively doped the sample until saturation was reached after ca. 15 h of doping. It was verified that the absorption of the iodine vapor in the optical cell is negligible with respect to that of the doped thin films.

Raman spectroscopy was performed on pristine and doped pentacene powders using a Krypton ion laser at a wavelength of 568.188 nm. The Raman scattering was analyzed by using a "Spex, Triplemate" monochromator 1879 coupled to a cooled CCD camera. The samples were investigated in the 180° backscattering mode using the toluene spectrum as a frequency calibration.

FT-IR measurements were performed by using a photoacoustic spectrometer based on a DigiLab FTS 7000 FTIR spectrophotometer coupled to a MTEC 300 photoacoustic detector (Photoacoustics Inc). The method is based on the comparison of the photoacoustic response of the sample with that of an infrared "blackbody".[21]

4. X-ray Diffraction. X-ray diffraction was performed on a Siemens D5000 diffractometer in (θ, 2θ) mode using Cu−K_α radiation ($\lambda = 1.5405$ Å). XRD acquisition was performed immediately after doping and weighting of the samples with an acquisition time of 30 min, a time scale during which the iodine loss by the sample is negligible (vide supra).

5. Electron Spin Resonance. The ESR experiments have been performed between 4 and 400 K with an ESP300 E or an ER200D spectrometer (BRUKER) operating at X-band (ca. 9.8 GHz) equipped with a TE102 rectangular cavity and an "Oxford" ESR900 cryostat. The temperature measurements were performed by inserting an AuFe/Chromel thermocouple close to the sample location. Quartz sample tubes were designed so as to allow in situ iodine insertion and pumping, as well as sample degassing. Care was taken to avoid signal distortion by over-modulation or microwave power saturation. The weak signals (thin films and single crystals) were accumulated as required. The spin concentration of single crystals and powders was assessed (within ca. 10−20% error) by weighting the samples and by calibration against a standard material (VARIAN pitch) with ESR parameters (line width, g-factor) similar to those of doped pentacene at RT.

6. Conductivity Measurements. The conductivity of pentacene single crystals doped with iodine was measured in the four probes geometry. Four gold contacts (interdigit distance of 600 μm) were deposited by thermal evaporation under vacuum. During deposition, the substrates were cooled at liquid nitrogen

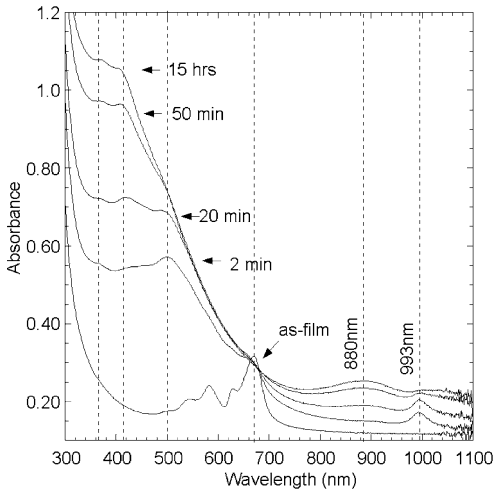

Figure 2. Evolution of the optical absorption spectra of a 50-nm-thick film of pentacene onto PTFE grown at $T_s = 70$ °C upon iodine doping from the vapor. The spectra have not been shifted along the ordinate axis. The progressive shift to higher absorbances is due to the increased reflectivity and scattering of the doped films (see text).

temperature to avoid structural damage by diffusion of gold in the bulk of the single crystals. The samples were mounted on a specific holder and the contacts were connected using thin gold wires fixed with silver paste. The measurements were carried out using a source measure unit, SMU 237, and a digital multimeter, DMM 2000, both from Keithley Instruments Inc. The conductivity was measured at room temperature and, in some cases, as a function of temperature, by cooling down to 77 K. The measurements of the conductivity of pentacene films were described in section II.3.

III. Results and Discussion.

A. Spectroscopic and Structural Evidences for Charge Transfer. In this section, we will successively describe the consequences of charge transfer on the optical and structural properties of the doped materials, that is, the spectroscopic evidences of the various polyiodides, the cationic species involving the cation radical PEN^+, the delocalized conduction electrons, and finally the crystal structure in doped single crystals.

1. Spectroscopic Signatures of the Various Species Formed upon Iodine Doping. Figure 2 depicts the evolution of the optical absorption spectrum of 50-nm PEN films grown onto oriented PTFE as a function of increasing doping time.

The undoped PEN films ($T_s = 70$ °C) exhibit the expected absorption spectra characterized by the vibronic progression with origin at 690 nm.[19] Upon doping, we observe the following modifications of the spectrum: (i) the disappearance of the undoped PEN absorption bands, (ii) the emergence of two narrow bands centered at 990 nm (A band) and 880 nm (B band), (iii) the development of a broad structured band in the range 300−600 nm, and (iv) an increase of the apparent absorption background. No significant change in the optical absorption spectra was observed for $t_d > 15$ h, indicating a saturation of film doping. Thus, according to previous results this doping time corresponds likely to I/PEN ≈ 6.

(a) Spectroscopic Signatures of Polyiodides. The first band appearing in the UV−vis spectra upon doping is centered at 500 nm and is attributed to molecular iodine.[11,22] This absorption loses its relative importance as the doping proceeds in favor of several other bands which are all related to charge-transfer events from iodine to pentacene, namely, the formation of

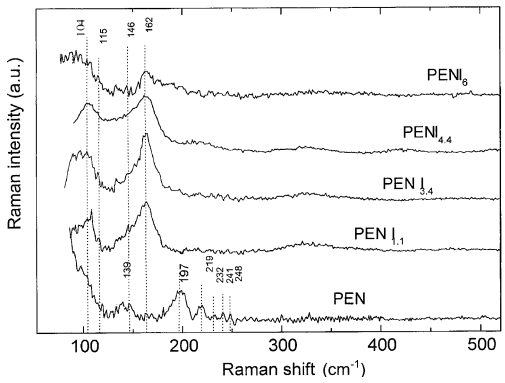

Figure 3. Evolution of the Raman spectrum of iodine-doped polycrystalline powders as a function of increasing concentration of iodine. For clarity, the spectra were shifted along the ordinate axis.

polyiodide ions, such as I_3^- and I_5^-, and the formation of cation radicals PEN^+. Polyiodides such as I_3^- and I_5^- are reported to show strong absorption bands between 360 and 430 nm.[23] The spectrum of Figure 1 exhibits two absorption components in this range (370 and 407 nm).[24]

Figure 3 represents the intensity of the Raman spectra of doped pentacene powders. For $1 \leq$ I/PEN ≤ 6, the spectra are qualitatively similar and demonstrate lines very typical of the polyiodide species,[25] mixed at low iodine concentration with the lines of the pristine pentacene.[26,27] The Raman spectra in Figure 3 are significantly different from that reported for perylene·$I_{2.92}$.[3] Deplano et al. have collected a large number of polyiodides, the structures and Raman spectra of which are reasonably well established.[25] The linear symmetric tri-iodide chain $(I-I-I)^-$ is expected to give a Raman peak around 110 cm^{-1}, whereas the asymmetric tri-iodide chains such as $I^-\cdot I_2$ is expected to yield a Raman peak at 167 cm^{-1}. Both these values agree fairly well with the observed peak positions in Figure 3, that is, 104 and 162 cm^{-1}, which are observed for all doped samples (see Figure 3).

Polyiodides with composition higher than I_3^- are usually found in the form of a combination between I^- or I_3^- with molecular I_2. For instance, I_5^- is either observed in the form of $I_3^-\cdot I_2$ or $I^-\cdot(I_2)_2$.[25] In the present case, we note the absence of a clear Raman peak corresponding to molecular iodine for $\nu_{I-I} \approx 200$ cm^{-1}. This implies that, regardless of the composition, the molecular iodine I_2 is always associated to either I^- or I_3^- to form polyiodides. The peak positions reported for I_5^- in the form $I_3^-\cdot I_2$, that is, 164, 135, and 106 cm^{-1}, are very close to the ones observed in our case, that is, 162 and 104 cm^{-1}. Only the peak at 135 cm^{-1} is not clearly visible in the present case. The comparison with (trimesic acid·$H_2O)_{10}\cdot H^+I_5^-$ is more pertinent since this compound shows two peaks similar to those in Figure 3 at 162 and 104 cm^{-1}.[24,25] In this latter material, I_5^- is described as a linear chain of the type $(I_2\cdot I^-\cdot I_2)$. These results suggest that the dominant polyiodides formed in doped pentacene correspond to linear chains of I_3^- and I_5^- which cannot be clearly distinguished in the present case.

It is also important to notice that some of the lines of the pure pentacene spectrum disappear as the doping proceeds. It is the case[27] for the intermolecular mode at 137 cm^{-1} and for the two intramolecular lowest frequency symmetric modes at 186 and 192 cm^{-1}. The X-ray diffraction spectra of §2 will also show the fading of the pristine structure, which disappears completely for I/PEN ≈ 2.

(b) Spectroscopic Signatures of Localized PEN^+ Cations and Related Species. The spectra in Figure 2 reveal absorption lines centered at 407 990 (A band) and 880 nm (B band). According

to Szczepanski et al.,[28] the pentacene cation radical PEN^+ is characterized by three absorption bands at 426, 946, and 842 nm. We therefore attribute the first two bands at 407 nm and 990 nm to the $^2A_u \leftarrow {}^2B_{1u}$ and the $^2A_g \leftarrow {}^2B_g$ transitions of isolated PEN^+ radicals, respectively. In ref 28, the 842-nm band has been attributed to a vibronic satellite of the $^2A_g \leftarrow {}^2B_g$ transition separated from the band origin by 1392 cm^{-1} which corresponds to the energy of the a_g C−C symmetric stretching mode.[28] In our case, the fact that the 880-nm band increases in intensity while the 990-nm band decreases and vanishes after 60 min of doping suggests a different origin of this band. Rather, the kinetics in Figure 2 supports a mechanism of conversion of the PEN^+ radicals in a different species giving rise to the absorption at 880 nm. In analogy with TTF-halide systems,[29,30] this new species corresponds very likely to dimers of the type $(PEN^+)_2$ which appear progressively as the concentration in PEN^+ cations increases with increasing iodine concentration. This hypothesis is further supported by the presence of dimers (nonequivalent molecules from a symmetry point of view) in the starting crystal structure of the undoped material.[20] Given the slipped-parallel configuration of the pentacene molecules in the bulk crystal structure of the pristine material, one would expect a blue shift (Davydov shift) of the dimer transitions with respect to the sole cation since the transition dipoles are parallel. The magnitude of the observed blue shift between the A and B bands, that is, 0.14 eV, is fully consistent with this picture of dimers. From the thermodynamic point of view, the formation of dimers is likely to be favored by Coulombic interactions between the two permanent dipoles of adjacent (PEN^+, I_x^-) pairs. The ESR measurements presented in the next section will further support the existence of localized PEN^+ cations and related clusters (dimers). The 880-nm band could also be related to PEN^{2+} cations. However, this assignment seems less relevant for two reasons, namely, (i) the lower probability of oxidizing twice the same molecule with a single electron transfer to iodine and (ii) the higher energetic cost.

Typical signatures of the PEN^+ cations are also visible in the IR spectra of Figure 4. The absorption was calculated by using a reference photoacoustic spectrum consisting of a black reference that absorbs nearly all the incident infrared light. Additionally, a smooth baseline was subtracted to facilitate the readout. Most lines appearing upon doping coincide with the vibrational modes of the radical PEN^+ obtained in previous spectroscopic studies on isolated PEN^+ ions in an argon matrix.[28,31,32] Table 1 lists the positions of the new lines and compares them to the vibrational absorptions of the isolated pentacene cations in the works of Szczepanski et al.[28] and Halasinski et al.[31] Most of these new lines are strongly coupled to the π-conjugated electron system. New peaks appear at 1964, 2553, 2728, and 2769 cm^{-1}, that is, within a spectral range where no pentacene peaks are expected. They can be attributed to overtones of the cation peaks.

(c) Scattering and Diffuse Reflectivity. The growth of the apparent absorption background in the visible and in the near UV is attributed to (i) the coarsening of the film morphology and (ii) the increase of the diffuse reflectivity upon doping.

The coarsening of the surface is clearly observed by AFM (see Figure 5) which evidences a significant increase of film roughness as well as a swelling of the pentacene microcrystallites upon doping with iodine, typically from 8 nm to 36 nm RMS roughness after 1 h of doping. It has to be stressed that the doped film morphology is clearly distinct from the pristine films which exhibit well-defined microcrystals with sharp edges and molecular terraces for $T_s \geq 70$ °C. Instead, the films

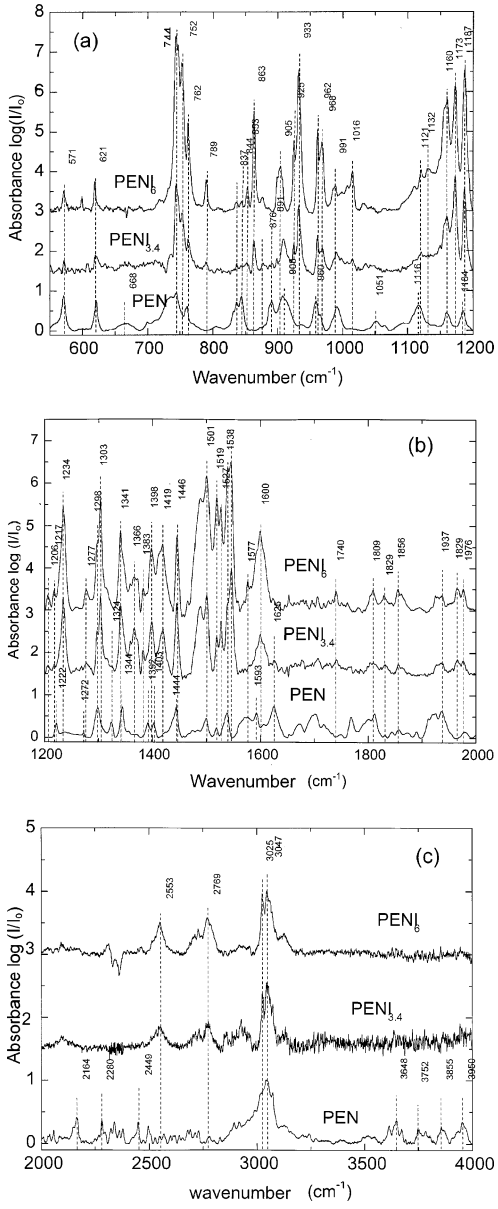

Figure 4. FT-IR spectra of pure and iodine-doped polycrystalline powders of pentacene. The spectral domain has been divided into three parts (a, b, and c). To compare the intensities of the vibrational modes, the baselines were subtracted and all spectra were renormalized to the intensity of the absorbance peak of the CH stretching vibration at 3047 cm^{-1} (see text). The new band frequencies related to doping are listed in Table 1. (I_0 represents here the response of the spectrometer to a blackbody reference).

obtained for a doping time $t_d = 15$ h show swollen domains without any indication for crystalline order, that is, no sharp edges and no terraces (see Figure 5). The coarsening of the film morphology is the main origin for scattering and diffuse reflectivity. The occurrence of charge transfer upon increasing doping time also enhances diffuse reflectivity and explains the rise of the background in the UV−vis domain. Diffuse reflectivity does not imply a metallic character of the films, which, in view of our ESR and conductivity measurements (vide infra), is not achieved in our samples (no evidence for a Drude edge is observed).

The increase of the background in the UV−vis domain is reproducible and reversible upon dedoping. Indeed, from a structural point of view, the initial morphology in terms of grain size and shape is recovered after dedoping with an RMS roughness almost identical to the pristine pentacene films.

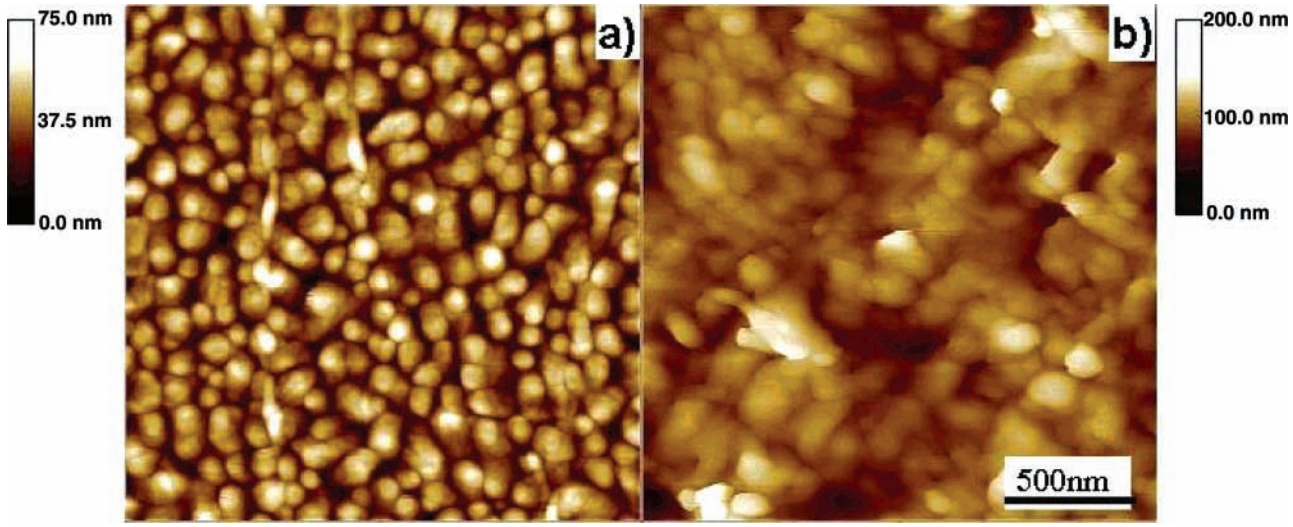

Figure 5. Comparison of the morphology of a 50-nm pentacene thin film deposited onto oriented PTFE at $T_s = 25$ °C before (a) and after (b) doping with an iodine vapor for 1 h. Please note the different scales for the *z* axes, underlining the important swelling of the pentacene domains by iodine.

TABLE 1: Principal IR Bands for Pen^+ Cations Observed in Doped Polycrystalline Pentacene Powders[a]

	υ (cm^{-1})	
I_2 doped power	cation (Szczepanski et al.)[b]	cation (Halasinski et al.)[c]
752		
789		
853		
925		
933	934	
1016		
1132		
1173	1174.9	
1234	1232.8	
1277		
1303	1306	
	1362	
1366	1365.8	
	1367.2	
1372	1372.5	
1398	1395.7	
1419	1417.9	1424, 1401, 1394*
1489	1487.8	
1526		
1545	1549.5	
1964		
2550		
2728		
2769		

[a] For comparison, the vibration frequencies of matrix isolated pentacene cations reported in other works are also listed. [b] Reference 28. [c] Reference 31.

However, the initial birefringence of the oriented pentacene films is lost after dedoping. Also, the terraces of the microcrystals are smeared out after dedoping. This suggests that the doping process is not strictly reversible from a structural point of view and significant disorder at the molecular scale is left in the microcrystallites after dedoping. The fact that the roughness of the films returns to its initial value after dedoping is consistent with our explanation for diffuse reflectivity and scattering.

The increase of diffuse reflectivity of the samples upon doping has also been observed in the IR range on polycrystalline powders. As the iodine concentration increases, the baseline of the unprocessed spectra (not shown) is significantly shifted in a reproducible way: the higher the concentration, the lower the overall apparent absorption. We attribute this effect to a broad increase of the IR reflectivity of the doped samples because of the existence of a variety of delocalized "band" excitations in the pentacene sublattice. Concomitantly, the apparent absorbances of intramolecular vibrations are seen to decrease because of the loss of incident infrared light by the increased reflectance of the sample.

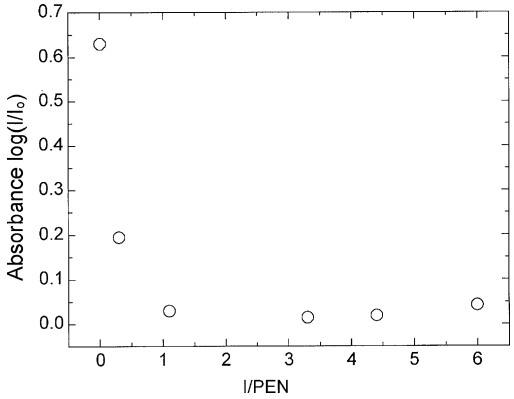

Figure 6. Absorbance of the pentacene C−H stretching mode at 3074 cm^{-1}, measured with respect to a blackbody, as a function of the doping concentration. The apparent absorption decrease is due to the increase of the IR reflectivity of the sample (see text).

To quantify this effect, we present, in Figure 6, the measured absorption of the CH stretching vibration at 3047 cm^{-1}. At I/PEN = 2, this absorption has reached its minimal value and does not change significantly upon higher doping concentration. The C−C stretching modes around 1400 cm^{-1} are the most sensitive to the doping process. Indeed, according to theoretical calculations,[33] these vibrations are strongly coupled to extra charges and here their sensitivity to doping witnesses the efficiency of the charge-transfer process.

2. Structure of Doped Materials. The spectroscopic experiments showed the buildup of polyiodide species, as they are entering the pentacene host structure. However, an important question with respect to the crystal structure has to be answered: where does the iodine go, and what do we know about its organization with respect to the pristine crystal structure of pentacene?

Figure 7 depicts the evolution of the X-ray diffractogram of a pentacene single crystal upon iodine doping. The initial structure of the single crystals is characterized by (0 0 *l*)

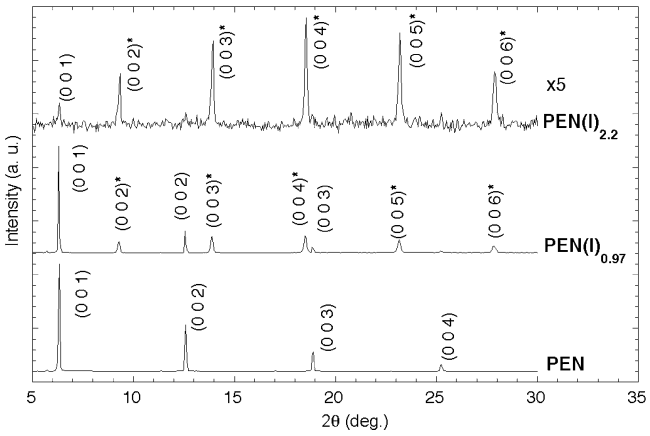

Figure 7. X-ray diffractograms of pure and doped pentacene single crystals. For $0.2 \leq$ I/PEN ≤ 2 iodine per pentacene, two lamellar structures coexist and correspond to the intercalate and the pristine pentacene. Peaks marked with a star correspond to the iodine intercalate.

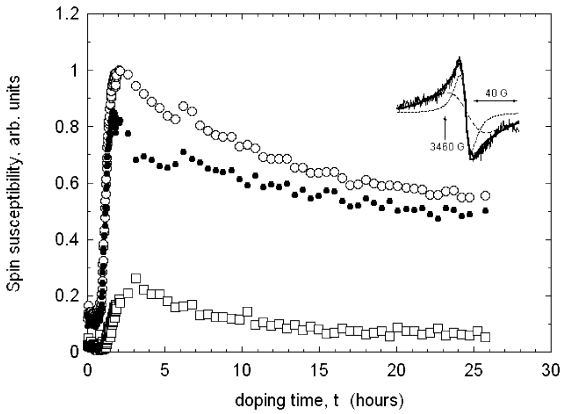

Figure 8. Room-temperature ESR spin susceptibility of a thin film (50 nm) as a function of the doping time (empty circles). The ESR line has been analyzed using two Lorentzian components as shown in the inset: a narrow one (empty squares) peak-to-peak width, $\Delta H_{pp} \approx$ 9 G centered at $g = 2.005$ and a broad one (filled circles) with $\Delta H_{pp} \approx 30$ G centered at $g = 2.004$.

reflections ($1 \leq l \leq 4$) with $c = 1.41 \pm 0.02$ nm and it corresponds to the structure determined by Holmes et al.[20] For I/PEN < 2, the samples consist of two phases: (i) the undoped material and (ii) an iodine intercalate characterized by (0 0 *l*)* reflections ($2 \leq l \leq 6$) as observed by Minakata et al.[12] This intercalate is characterized by $c = 1.82 \pm 0.04$ nm which corresponds to the sum of the width of the pentacene layer (1.41 nm) plus the van der Waals diameter of the intercalated iodine layer (0.43 nm). This observation suggests that I_3^- and I_5^- polyiodide chains evidenced by Raman spectroscopy are lying parallel to the (*a*,*b*) planes of the pentacene single crystals. The intensity of the nonintercalated pentacene structure is progressively decreasing at increasing iodine concentration until the concentration of I/PEN $\cong$ 2.2 is reached. At I/PEN > 2.2, the intensity of the intercalated compounds also decreases. It disappears for the heavily doped samples of composition I/PEN = 5.7.

Assuming that iodine is organized in the form of a close-packing of tri-iodide chains, we can derive a composition of the intercalate $PEN(I)_{1.82}$ which changes to $PEN(I)_{2.0}$ for close-packed polyiodide chains of infinite length.[35] Accordingly, samples with I/PEN > 2.0 do not correspond to intercalates and the iodine must also be present within the (*a*,*b*) layers of the pristine structure. Then, the polyiodide phase is hosted within a tridimensional mode of organization, and the unsolved X-ray diffraction pattern supports the picture of a disordered phase.

These facts, strengthened by the indications from other experiments, will have important consequences. From zero to approximately one iodine atom per pentacene, part of the lamellae of the doped pentacene crystal maintain the same electronic structure as pristine pentacene, with an in-plane bandwidth of about 0.8 eV.[36] Holes are transferred to these high mobility zones. However, these charges are not necessarily tightly bound to the polyiodide. This will result in electrical conduction, Pauli susceptibility contribution, and infrared and visible light reflectivity. As the raise of the iodine ion concentration is leading to a more tridimensional and disordered polyiodide structure, this will in turn favor the localization of holes by increasing the correlations between the polyiodide counterions and the transferred holes on the pentacene lattice. Evidences for these localization processes will be given in part B where the results of ESR experiments are discussed.

B. Magnetic Signature of Charge Transfer and Transport Properties. The spectroscopic investigations of doped pentacene in section A have demonstrated the efficiency of charge transfer between iodine aggregates and pentacene molecules (or clusters). The increase of the overall reflectivity was the reason to suspect the presence of holes delocalized over pentacene layers, while visible and infrared lines were assigned to the possible existence of localized hole radicals (PEN^+) and dimers $(PEN^+)_2$. These species are clearly assigned in the following section through electron spin resonance (ESR) experiments and electrical conductivity measurements.

1. Electron Spin Resonance (ESR). There is no ESR signal in the pristine pentacene. The presence of an ESR line at *g* close to the free electron *g*-value in doped samples is thus the consequence of the presence of unpaired holes on the pentacene molecules. In turn, the presence of different types of counterions (I^-, I_2^-, I_3^-, I_5^-, etc.) located in various parts of the materials and more or less correlated to the holes creates the conditions for a large variety of spin behaviors in the doped materials. The ESR response of powders, thin films, and single crystals has been studied at various doping stages. The kinetics of iodine doping has been recorded at room temperature for the various samples. Besides the investigation of the doping mechanism that these studies could allow, they have been used to calibrate the iodine content of the conductivity experiments. The analysis of the temperature dependence of the ESR spin susceptibility favored the emergence of a common qualitative picture valid for all samples. Accordingly, it was possible to classify the spin behaviors according to three types of spin susceptibility and two types of ESR line shapes. These are closely related to three doping regimes defined from the structural and spectroscopic investigations: low iodine content (I/PEN < 0.05), intermediate range (0.2 < I/PEN < 2), and high doping range (I/PEN > 5).

(a) Doping Kinetics and ESR Line Shape. The inhomogeneous character of the spin population is also reflected in the ESR line shape which appears as composed of at least two contributions: a broad one and a narrow one, as already observed in the work of ref 17 for potassium doped pentacene. In the limiting case of the lightly doped single crystal (I/PEN < 0.05) of Figure 9a, we have recorded a single Lorentzian line centered at $g = 2.003$ with a peak-to-peak line width $\Delta H_{pp} \sim 1.5$ G over the whole temperature range. The anisotropy of the ESR signal of this single crystal indicates a periodic angular dependence of the *g*-tensor within the (*a*,*b*) plane, thus confirming that the crystal structure is not significantly distorted in the low doping regime. This narrow component appears somewhat broader (half-width at half-maximum, $\Delta H_{1/2}$: 3 to 4 G) in the powder and in single crystals at higher doping concentrations.

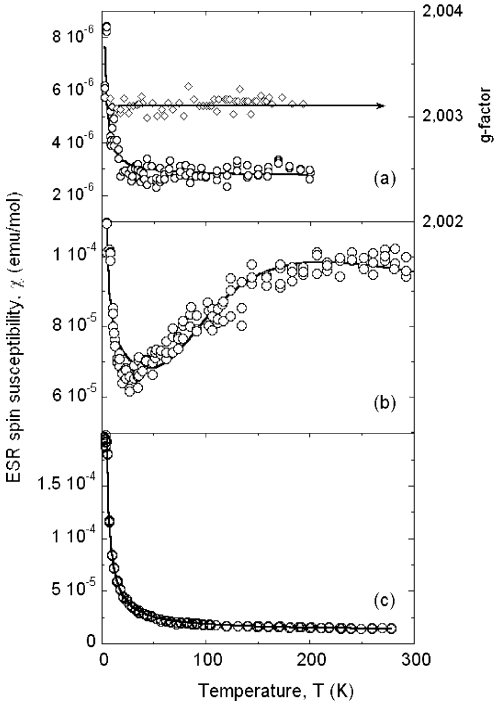

Figure 9. ESR spin susceptibility of doped pentacene: (a) single crystal for I/PEN = 0.05; (b) polycrystalline powder for I/PEN = 1; (c) polycrystalline powder for I/PEN = 5.98. Continuous lines are the results of the fits using eq 1.

The broad component ($\Delta H_{1/2} = 8 \sim 12$ G, and up to 30 G in thin films) is centered at $g = 2.004-2.007$ depending on the sample and on the temperature. This higher value of g reflects the presence of heavy iodine ions at the proximity of these latter spins, which shifts the free electron line through spin−orbit coupling. Indeed, the broad line corresponds to spins which are more correlated to the iodine ion species from which they originate. It is thus natural to attribute the narrow component to more delocalized holes and the broad component to more localized species, especially radical cations and related clusters.

Figure 8 represents the evolution of the ESR intensity of the two lines as the doping proceeds in thin films. We observe that the total magnetic susceptibility reaches a maximum after a few hours of doping and then decreases again. In terms of induced Pen^+ radical per iodine, we observe that it never exceeds 5−6%, indicating that most spins are ESR-silent.

The time dependence of the ESR susceptibility in Figure 8 suggests the following mechanism of doping. First, Pen^+ radicals are randomly generated in the samples and their concentration increases upon increasing doping. The low value of the slope for the linear dependence with iodine concentration is certainly due to (i) the inhomogeneous doping in the sample (preferentially the surface) as well as (ii) the solvation barrier that must be overcome to induce doping. As the spin concentration is further increased, cation dimers $(Pen^+)_2$ and related species are formed. Given the inhomogeneous character of the doping process, it is certain that larger spin clusters of different sizes but with dominant antiferromagnetic correlations do also contribute to the magnetic behavior, so that the apparent ESR susceptibility decreases with increasing iodine doping. Finally, the spin susceptibility reaches a plateau at high doping which corresponds mainly to a population of localized spins as shown in the following.

(b) Temperature Dependence of the Magnetic Susceptibility. The overall ESR picture presents significant similarities with the work of ref 17 performed on potassium-doped pentacene, although we consider here a broader doping range and several types of materials including single crystals and oriented polycrystalline thin films.

A common qualitative picture could be drawn from the overall results obtained on the different samples, as illustrated in Figure 9. At very low iodine content (I/PEN < 0.05), the spin susceptibility is almost constant with temperature, being of the Pauli type except for a small Curie tail at low temperature. At intermediate doping ($0.2 \leq$ I/PEN ≤ 1), the susceptibity is dominated by a thermally activated behavior whereas for the high doping range (I/PEN ≥ 5) a Curie-like behavior is observed. Accordingly, the spin susceptibility was modeled with three-components, a Pauli susceptibility, a Curie component, and a thermally activated component typical for a singlet−triplet equilibrium as given in the following equation:

$$\chi = \chi_P + \frac{C_1}{T} + \frac{C_2}{T}\left(\frac{4}{3 + \exp(-T_0/T)}\right) \qquad (1)$$

(i) Low Iodine Concentration (I/PEN ≤ 0.05). In the low iodine limit (I/PEN ≤ 0.1), the pristine structure of pentacene is maintained (see section III, A.4) and the high reflectivity of the samples suggests that delocalized holes are formed by charge transfer between iodine and the valence band of pentacene. Accordingly, the Pauli-like contribution, χ_P, is considered as originating from these delocalized holes.

The value of $\chi_P \sim 3 \times 10^{-6}$ emu/mol visible on Figure 9a concerns a single crystal at doping concentrations lower than 0.05 iodine atom per pentacene. In this range, the Pauli contribution looks essentially independent of the doping concentration (see Table 2). The observed value of χ_P is comparable to previous estimations of a Pauli-like susceptibility in iodine[14] or in potassium heavily doped[17] pentacene.

If we assume that χ_P is essentially due to a 2-D electron gas delocalized within the pentacene layers of the pristine (undoped) structure, the order of magnitude of χ_P and its independence with respect to the concentration can be predicted theoretically from the well-known Pauli susceptibility per mole for a 2-D electron gas:[37]

$$\chi_P = \mu_B{}^2 N/2\Delta E \qquad (2)$$

With the bandwidth of 0.8 eV of ref 36 we can estimate the order of magnitude of χ_P of 2×10^{-5} emu/mol, that is, corresponding to a density of states at the Fermi level of the order of 0.3 states/eV·PEN for both spin polarizations. In the present low doping range, the estimated values of χ_P are 1 order of magnitude lower than this estimation. This is again attributed to the highly inhomogeneous character of doping: large parts of the samples are undoped as evidenced through XRD.

The estimated Curie constant (per mole of pentacene) $C_1 = Nx_1\mu_B{}^2/k_B$, where k_B is the Boltzmann constant and x_1 is the fraction of pentacene radicals, is about 10^{-5} emu·K/mol. Related to $S = 1/2$ localized spins, it corresponds to a molecular fraction x_1 of radicals about a few 10^{-5}.

In addition to the previous two components of the susceptibility, the low temperature behavior of samples with I/PEN = 0.03 and I/PEN = 0.053 requires a third contribution for a satisfactory fit. For the sake of consistency with the procedure adopted in the next section (intermediate doping range), a thermally activated contribution has been used. The obtained activation energy is about 20−30 K, that is, much lower than reported for intermediate doping (see below).

(ii) Intermediate Doping Range (0.2 ≤ I/PEN ≤ 1.0). A thermally activated behavior is clearly observed at intermediate

TABLE 2: Parameters Obtained from the Fitting of the ESR Susceptibility of Iodine-Doped Single Crystals and Powders of Pentacene ($0.01 \leq$ I/PEN ≤ 5.98) Using eq 1 Given in the Text

		x (PEN-I$_x$)	χ_0 (emu/mole PEN)	C_2 (spin pairs/PEN)	T_0 (K)	C_1 (emu/mol PEN)
crystal	low doping	0.015	$(2.8 \pm 0.1) \times 10^{-6}$			$(3.5 \pm 0.3) \times 10^{-5}$
		0.030	$(3.9 \pm 0.2) \times 10^{-6}$	$(2.4 \pm 0.2)\ 10^{-4}$	(29 ± 2)	$(1.8 \pm 0.5) \times 10^{-4}$
		0.053	$(3.0 \pm 0.1) \times 10^{-6}$	$(2.0 \pm 0.1)\ 10^{-4}$	(21 ± 1)	
powder	intermediate doping	0.21	$(10.6 \pm 0.1) \times 10^{-6}$	$(1.1 \pm 0.5)\ 10^{-3}$	(373 ± 13)	$(7.7 \pm 0.8) \times 10^{-5}$
		1.0	$(63 \pm 9) \times 10^{-6}$	$(2.0 \pm 0.1)\ 10^{-2}$	(344 ± 9)	$(5.3 \pm 0.3) \times 10^{-3}$
	high doping	5.25	$(44 \pm 1) \times 10^{-6}$	$(6.0 \pm 0.1)\ 10^{-3}$	(487 ± 35)	$(7.7 \pm 0.8) \times 10^{-3}$
		5.98	$(9.8 \pm 0.3) \times 10^{-6}$	$(1.2 \pm 0.1)\ 10^{-3}$	(383 ± 20)	$(2.0 \pm 0.1) \times 10^{-2}$

doping range in powders (Figure 9b). According to the results gained from optical spectroscopy, this third contribution may be attributed to the presence of dimers of the type $(Pen^+)_2$. Therefore, its temperature dependence is expressed as a singlet−triplet equilibrium. The susceptibility data corresponding to single crystals and powders have been fitted to eq 1 and the corresponding fitting parameters are reported in Table 2. The value of C_2 per pentacene mole ($C_2 = 2Nx_2\mu_B^2/k_B$) yields a fraction x_2 of independent spin pairs per pentacene molecule about $10^{-3}-10^{-2}$. The singlet−triplet gap, T_0, gained from the various fits yields a mean value of 359 ± 20 K.

It has, however, to be stressed that the overall temperature dependence of the spin susceptibility in this doping range is very similar to that observed, for instance, in antiferromagnetic 1-D chains consisting of an odd number of spins, as demonstrated by Fisher and Bonner.[38] Accordingly, and in the light of the disordered nature of the iodine in the samples, we may also attribute the temperature dependence of the susceptibility to spin clusters with a given distribution of sizes. In this perspective, the various T_o values obtained from the fitting with eq 1 may simply reflect the evolution of the size distribution of spin clusters with increasing doping in the samples.

From the estimated Curie constant C_1, the molecular fraction x_1 of $S = 1/2$ localized spins is ranging between a few 10^{-5} to a few 10^{-3}. As for the low doping stage in single crystals, this again has to be noticed as being very small with respect to the concentration of iodine in this intermediate range, indicating that most spins are paired and ESR-silent.

(iii) High Doping Range (5 ≤ I/PEN). At high iodine content, the Curie contribution is dominating the spin susceptibility (Figure 9c). We attribute it to the presence of localized pentacene cation radicals.

The fraction x_1 (eq 1) of localized spins does not vary appreciably for $1 \leq$ I/PEN ≤ 6. Again, this number is very small with respect to the doping concentration. A Pauli-like susceptibility is still present at this stage, being of the same order as in the previous range.

The estimated spin concentrations of localized spin species in the different samples are always 3 orders of magnitude lower than the iodine content. It is inferred that most of the spins are paired and do not contribute to the ESR spin susceptibility in this temperature range. Such a broad distribution of spin clusters and T_0 values gives very often a final contribution to the spin susceptibility rather constant over a broad range of temperatures as observed in disordered carbons[39] and in disordered doped conducting polymers.[40,41] Accordingly, the Pauli contribution that is gained from the fit, when the sample is highly disordered, is probably not related to the conduction electrons evidenced at low doping.

In conclusion, both by analyzing the temperature dependence of the spin susceptibility and by studying the ESR line shape, we have shown the existence of a broad distribution of spin carriers which can be roughly divided into two classes: (i) the more localized ones, radicals, dimers, and more complex spin clusters significantly correlated to iodine ions from which they originate and (ii) a minority of more delocalized ones which, at least at low doping, are transferred to the pentacene valence band and contribute to a narrow line and a Pauli susceptibility.

2. Conductivity Measurements. Homogeneity is even more important in conductivity measurements than in any other experiment because four probe measurements in a planar configuration are very sensitive to the existence of a dopant accumulation at the surface.

For these reasons, we have only used very thin single crystals (from 50 to 70-nm thick) and very low doping kinetics (less than 1% I/PEN per hour). The validation of our results comes mainly from the fact that the same results are obtained for single crystals as for 50-nm polycrystalline films grown on PTFE.

In all samples, whatever the crystallinity (thin film, pressed powder, single crystal), the conductivity values never exceed a few S·cm^{-1} at room temperature. The similar behavior is also observed for all samples as the doping proceeds: a conductivity maximum is observed by ca. I/PEN $= 3 \sim 4$, followed by a continuous decrease (Figure 10).

In Figure 11, a first conductivity measurement is presented on thin films of 50 nm, grown on oriented PTFE substrates at different T_s. In this case, the doping kinetic is fast and the doping is homogeneous through the whole film thickness. In ref 19, the electron diffraction patterns of similar films elaborated at different substrate temperatures T_s were given. The correlation between the conductivity values and the diffraction pattern is obvious: the higher the cristallinity of the pristine film, the lower the conductivity that can be obtained by doping. This implies that the doping process takes advantage from the structural defects, grain boundaries, stacking faults, and so forth. What is also important is the decrease of the conductivity at increasing iodine concentration above I/PEN > 3. In the same Figure 11, we have reported the spin susceptibility of a similar film determined by double integration of the ESR line at room temperature. We clearly see that the onset of conductivity decrease corresponds closely to the onset for the decrease of the total ESR susceptibility of the films. We attribute these observations to the increasing role of disorder at very high doping levels which is believed to lower the mobility of the charges in the system.

Figures 10 and 12 concern the conductivity of slowly doped single crystals; here, the samples have been weighted before the measurements and the iodine concentrations are known. Except at very low doping concentrations, the conductivity of doped pentacene is essentially temperature independent (within 1 order of magnitude) between 100 K and 300 K. According to the ESR results, the conductivity probes the simultaneous propagation of two types of carriers: a majority of localized holes moving by hopping from site to site and a minority of more delocalized holes. The presence of a conductivity minimum in the temperature dependence of samples doped at I/PEN > 1 reflects the competition between these two mechanisms: hopping at high temperatures and diffusion of more coherent

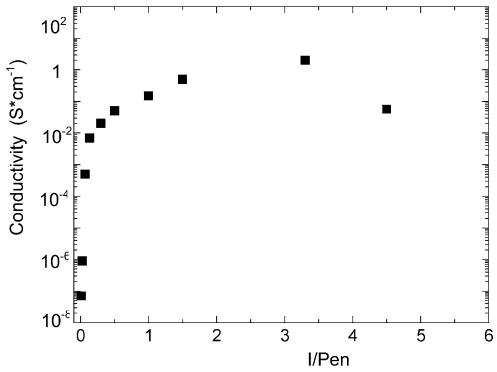

Figure 10. The conductivity of doped pentacene single crystals was measured as a function of the iodine concentration, I/PEN, determined by weighting the samples.

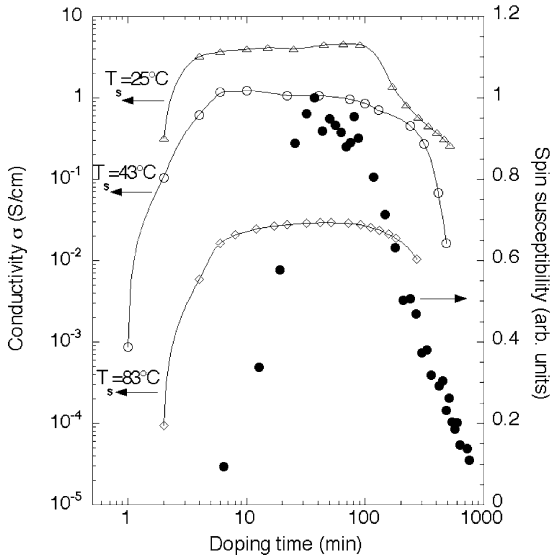

Figure 11. Evolution of the conductivity in pentacene thin films grown on oriented PTFE with increasing exposure time to an iodine vapor. The films have been grown at different substrate temperatures in the range 25−83 °C. The time dependence of the ESR signal intensity is plotted on the same graph.

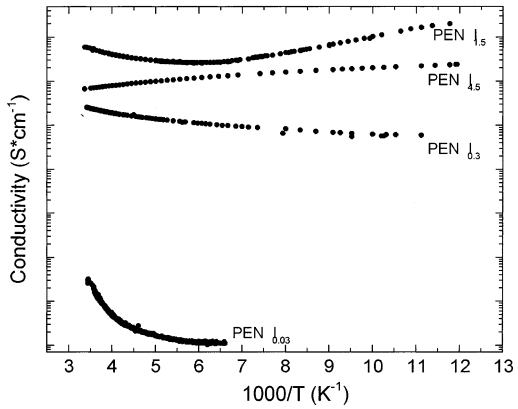

Figure 12. Conductivity versus temperature curves measured between 90 and 300 K for doped pentacene single crystals for different compositions in the range $0.3 \leq$ I/PEN ≤ 4.5.

carriers at low temperatures.[42] Moreover, the sample is heterogeneous at low doping concentrations and disordered at high doping concentrations. Thus, the resistance versus temperature curves resemble very much those of impure graphites, and the conductivity measurements only give access to general trends and not to detailed mechanisms.

IV. Conclusion

This work has demonstrated the existence of three distinct doping regimes. In the low doping regime I/PEN < 0.05, the structure of the pristine pentacene is maintained and the charge transfer from pentacene to iodine involves the formation of delocalized holes in the valence band of the narrow gap pentacene crystal. These delocalized holes are mainly characterized by a typical Pauli susceptibility.

In the intermediate doping regime $0.2 \leq$ I/PEN ≤ 2, an intercalate is formed which coexists to some extent with undoped PEN regions in the crystals. UV−vis and IR spectroscopies witness the existence of localized PEN^+ cations and possibly $(PEN^+)_2$ dimers which are formed at increasing iodine concentration. Spin pairing between pentacene cation radicals is further supported by a thermally activated susceptibility with an activation energy in the range 350−400 K, which depends on the size distribution of the spin clusters, that is, with the doping level. In this regime, Raman spectroscopy indicates that the dominant polyiodide species consist of linear chains of I_3^- and I_5^-.

In the high doping regime, that is, for I/PEN > 2, iodine penetrates the (*a*,*b*) planes of pentacene in a disordered manner. This situation is primarily due to the doping dynamics, which does not favor the setup of sufficient order in the polyiodide phase. Disorder is the condition for increased charge localization underlined by a dominant Curie magnetic susceptibility and a limited conductivity which does not exceed few $S \cdot cm^{-1}$.

The consequence of the buildup of the "polyiodide glass" is, on the one side, the possibility of iodine partial desorption and, on the other, hole trapping close to the less mobile ionic species of the polyiodide.

Acknowledgment. M. Bernard, C. Chaumont, M. Longchamp, and C. Straupé are acknowledged for their precious help and technical support. We thank H. Berger for his fruitful advice concerning single-crystal preparation. We received the help of the Swiss Federal Science Foundation under contract number 20-67929.02. Part of this work has been financially supported by an EU Program "Marie Curie Doctoral Training Site: *Chemical Synthesis and Electron Paramagnetic Resonance of Molecular Magnets*—Contract Number: HPMT-2000-00083". V. S. Videva was awarded a one-year fellowship within this EU program.

References and Notes

(1) Warta, W.; Karl, N. *Phys. Rev. B* **1985**, *32*, 1172.

(2) Kommandeur, J.; Hall, F. R. *J. Chem. Phys.* **1961**, *34*, 129. Singer, L. S.; Kommandeur, J. *J. Chem. Phys.* **1961**, *34*, 133.

(3) Teitelbaum, R. C.; Ruby, S. T.; Marks, T. J. *J. Am. Chem. Soc.* **1979**, *101*, 7568.

(4) Schramm, C. J.; Scaringe, R. P.; Stojakovic, D. R.; Hoffmann, B. M.; Ibers, J. A.; Marks, T. J. *J. Am. Chem. Soc.* **1980**, *102*, 6702.

(5) Martinsen, J.; Greene, R. L.; Palmer, S. M.; Hoffmann, B. M. *J. Am. Chem. Soc.* **1983**, *105*, 677.

(6) Ogawa, M. Y.; Martinsen, J.; Palmer, S. M.; Stanton, J. L.; Tanaka, J.; Greene, R. L.; Hoffmann, B. M.; Ibers, J. A. *J. Am. Chem. Soc.* **1987**, *109*, 1115.

(7) Warmack, R. J.; Callcott, T. A.; Watson, C. R. *Phys. Rev.* **1975**, *B12*, 3336.

(8) Kilitziraki, M.; Moore, A. J.; Petty, M. C.; Bryce, M. R. *Thin Solid Films* **1998**, *335*, 209.

(9) Somoana, R. B.; Yen, S. P. S.; Hadek, V.; Khanna, S. K.; Novotny, M.; Datta, T.; Hermann, A. M.; Woollam, J. A. *Phys. Rev.* **1978**, *B17*, 2853.

(10) Simon, J.; André, J. J. *Molecular semiconductors*; Springer-Verlag: Berlin, Heidelberg, New York, Tokyo, 1985.

(11) Minakata, T.; Nagoya, I.; Ozaki, M. *J. Appl. Phys.* **1991**, *69*, 7354.

(12) Minakata, T.; Imai, H.; Ozaki, M. *J. Appl. Phys.* **1992**, *72*, 4178.

(13) Mori, T.; Ozaki, M.; Ikehata, S. *Solid State Commun.* **1993**, *88*, 203.
(14) Mori, T.; Ikehata, S. *Mater. Sci. Eng.* **1997**, *B49*, 251.
(15) Matsuo, Y.; Sasaki, S.; Ikehata, S. *Synth. Met.* **2001**, *121*, 1383.
(16) Mori, T.; Ikehata, S. *J. Appl. Phys.* **1997**, *82*, 5670.
(17) Mori, T.; Ikehata, S. *Solid State Commun.* **1997**, *101*, 213.
(18) Matsuo, Y.; Sasaki, S.; Ikehata, S. *Synth. Met.* **2003**, *137*, 955.
(19) Brinkmann, M.; Graff, S.; Straupé, C.; Wittmann, J. C.; Chaumont, C.; Nüesch, F.; Aziz, A.; Schaer, M.; Zuppiroli, L. *J. Phys. Chem. B* **2003**, *107*, 10539.
(20) Holmes, D.; Kumaraswamy, S.; Matzger, A. J.; Vollhardt, P. C. *Chem. Eur. J.* **1999**, *5*, 3399.
(21) McClelland, F.; Jones, R. W.; Luo, S.; Seaverson, L. M. *A practical guide to FTIR photoacoustic spectroscopy.* In *Practical Sampling Techniques for Infrared Analysis*; Coleman, P. B., Ed.; CRC Press: Boca Raton, FL, 1993.
(22) Tamres, M.; Bhat, S. N. *J. Phys. Chem.* **1971**, *75*, 1057.
(23) Fornier de Violet, P.; Bonneau, R.; Joussot-Dubien, J. *J. Chim. Phys.* **1975**, *72*, 855.
(24) All of these attributions result from the comparison of measurements reported in the literature, performed in water or in acetonitrile, to experiments here performed in a vacuum or in the solid state. Obviously, the solvation effects on the exciton have not been considered in detail and can explain the shift in position of some bands. We have here assumed that these effects give rise to corrections lower than 300 cm^{-1} to 500 cm^{-1}, and that they do not affect qualitatively our attributions, especially when Raman peaks confirm the presence of absorption peaks.
(25) Deplano, P.; Ferraro, J. R.; Mercuri, M. L.; Trogu, E. F. *Coord. Chem. Rev.* **1999**, *188*, 71.
(26) Rumi, M.; Zerbi, G.; Müllen, K.; Müller, G.; Rehahn, H. *J. Chem. Phys.* **1997**, *106*, 24.
(27) Brillante, A.; Della Valle, R. G.; Farina, L.; Girlando, A.; Masino, M.; Venuti, E. *Chem. Phys. Lett.* **2002**, *357*, 32.
(28) Szczepanski, J.; Wehlburg, C.; Vala, M. *Chem. Phys. Lett.* **1995**, *232*, 221.
(29) Scott, B. A.; La Placa, S. J.; Torrance, J. B.; Silverman, B. D.; Welber, B. *J. Am. Chem. Soc.* **1977**, *99*, 6631.
(30) Torrance, J. B.; Scott, B. A.; Welber, B.; Kaufman, F. B.; Seiden, P. E. *Phys. Rev. B* **1979**, *19*, 730.
(31) Halasinski, T. M.; Hudgins, D. M.; Salama, F.; Alamandola, L. J.; Bailly, T. *J. Phys. Chem. A* **2000**, *104*, 7484.
(32) Barbara, P. F.; von Borczyskowski, C.; Casalegno, R.; Corval, A.; Kryschi, C.; Romanowski, Y.; Trommsdorff, H. P. *Chem. Phys.* **1995**, *199*, 285.
(33) Coropceanu, V.; Malagoli, M.; da Silva Filho, D. A.; Gruhn, N. E.; Bill, T. G.; Bredas, J. L. *Phys. Rev. Lett.* **2003**, *89*, 275503.
(34) Kato, T.; Kondo, M.; Yoshizawa, K.; Yamabe, T. *Synth. Met.* **2002**, *126*, 75.
(35) *Handbook of Chemistry and Physics*, 53rd ed.; Weast, R. C., Ed.; CRC Press: 1972−1973; pp D-146/F-180.
(36) Cheng, Y. C.; Stilbey, R. J.; da Silva Filho, D. A.; Calbert, J. P.; Cornil, J.; Bredas, J. L. *J. Chem. Phys.* **2003**, *118*, 3764.
(37) Kittel, C. *Introduction to Solid State Physics*, 7th ed.; J. Wiley & Sons: New York, 1996.
(38) Bonner, J. C.; Fisher, M. E. *Phys. Rev. A* **1964**, *135*, 640.
(39) Salvetat, J. P.; Constantini, J. M.; Brisard, F.; Zuppiroli, L. *Phys. Rev. B* **1997**, *55*, 6238.
(40) Bussac, M. N.; Zuppiroli, L. *Phys. Rev. B* **1993**, *47*, 5493.
(41) Chauvet, O.; Paschen, S.; Bussac, M. N.; Zuppiroli, L. *Europhys. Lett.* **1994**, *26*, 619.
(42) Karl, N. *Synth. Met.* **2003**, *133*−*134*, 649.